

Motor Mode Analysis of Exterior-Rotor PM Machine with Gramme's Winding

Rene Nukki^{1,2}, Aleksander Kilk¹, Samo Saarts², Kristjan Tiimus Sr³
¹*Department of Electrical Engineering, Tallinn University of Technology,
 Ehitajate St. 5, 19086 Tallinn, Estonia*
²*Chair of Electrical Engineering, TTK University of Applied Sciences,
 Parnu St. 62, 10135 Tallinn, Estonia*
³*HeliCam Services Ltd.
 Looduspargi St. 4, 76901 Tabasalu, Estonia
 renenukki@gmail.com*

Abstract—This paper presents the PM electrical machine with the novel stator geometry, which is intended for a small unmanned aircraft. The PM machine is a part of a hybrid propulsion system operating in conjunction with an internal combustion engine. The main study involves operations in the motor mode, where the PM electric machine performs as the main propulsion, as well as the additional power source or a starter in the hybrid drive. The purpose of the investigation is experimental evaluation of the electric parameters of the PM electric machine in the motor mode; in particular, achievable torque at different speeds on several loads, to compare the results with the initial requirements.

Index Terms—Electric motors, permanent magnet machines, propellers, temperature dependence, testing.

I. INTRODUCTION

Today small unmanned aerial electric vehicles (UAV) are used for a wide range of purposes, like wildlife tracking, traffic monitoring, border patrols, environmental research, geographical mapping, numerous military applications and several more [1]. The reason for the increasing trend in the use of UAVs is their simple construction, reliability, easy operation, relative safety and environmental friendliness. The market of electric UAV market has grown into a multi-billion dollar industry [1].

Electric machines (EM) are also used in the UAVs that use an internal combustion engine (ICE) as their main source of power. In the named combination EMs are used mainly as generators. Lately hybrid propulsion systems (HPS), which have proven itself in the land and in the maritime transport [2] have started to expand into the field of UAVs. An HPS is generally an integrated single system, which uses two or more different power sources to move the vehicle. ICE's, also electric motors, have certain strengths and weaknesses. An HPS combines the strengths of both types of motors [2].

Nowadays interior, exterior and axial rotors are mainly used in electric-powered vehicles (Fig. 1) [3].

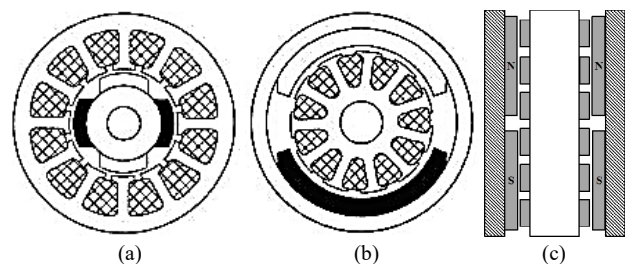


Fig. 1. Three basic machine configurations used in small UAV-s [3]: a – interior-rotor; b – exterior-rotor; c – axial rotor.

In this paper, the exterior-rotor geometry is selected. The novelty of the research lies in implementation of a new type of stator geometry in the exterior-rotor permanent magnet synchronous machine (ERPMSM) in combination with Gramme's or toroidal winding, also in usage of this kind of ERPMSM in a motor, as well as in a generator operation in an HPS for a small-size UAV.

The principle scheme of the novel HPS is shown in Fig. 2.

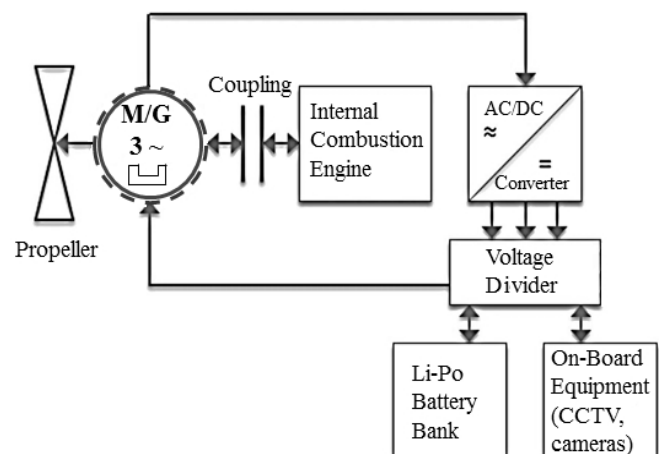


Fig. 2. Principle scheme of the UAV hybrid propulsion and energy storage system [4].

The choice of the ERPMSM's topology was determined by basic requirements, such as simple construction, low cost, high power-to-weight and power-to-volume ratio, smallest size, good control options and high torque at low speed. In this case, the exterior-rotor topology has several advantages. One example is the possibility to install additional

components into the internal opening of the stator, thus obtaining more compact solutions. For ERPMSM it is the mechanical clutch, which connects and disconnects ICE from it, which is rather complicated with the axial and interior-rotor design [4].

The other advantages of the exterior-rotor topology comparing for example with the interior-rotor design are higher torque density, better cooling possibilities, reduced copper loss, lower weight and cost [1].

ERPMSM solution is novel in its geometry and functionality as the same EM can be used as a motor and a generator. The operation in the generator mode was discussed already in the previous phase of the research [5]. In this study the main focus is on the ability of ERPMSM to work as a motor. This includes its capability to function as a primary engine which directly rotates a propeller, also operates in parallel with ICE as a starter or giving extra power during UAV's take off.

During the research the prototype of ERPMSM was also constructed (Fig. 3).

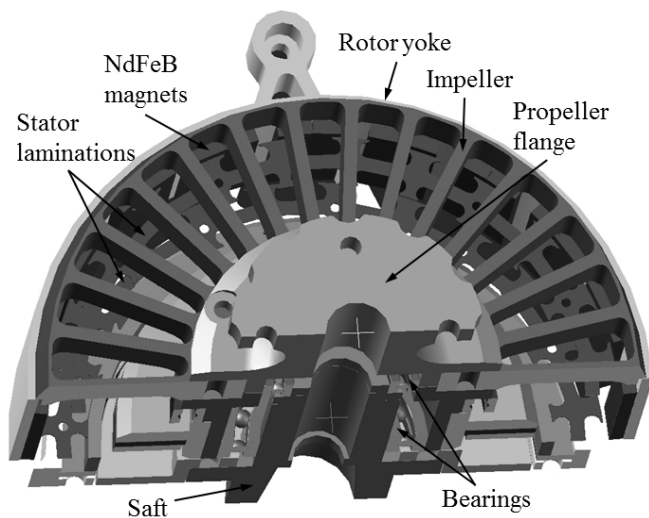


Fig. 3. The section geometry of the exterior-rotor motor-generator with the toroidal winding.

II. INITIAL PARAMETERS

One of the first initial design parameters for the HPS was the range of rotational speed between 3000 rpm to 4000 rpm, which meets the efficient operational regime of the propeller at UAVs stable flight situation.

An additional important nuance considered when ERPMSM functions as a motor, was the ability to output enough torque at required speeds of rotation while driving the propeller whilst maintaining the desired thermal parameters.

Various supplementary design parameters were given from ICE technical data, including the starting torque that ERPMSM had to overcome. In addition, manufacturer's requirement for the UAV is to be able to maintain stable flight for minimum of 15 minutes on electric power.

III. LOAD TESTS

During load tests of ERPMSM in motor regime, UAVs actual wooden propeller with the diameter of 508 mm and pitch of 355.6 mm was used as a load [7].

In Fig. 4, the counter torque of the propeller T_{pr} characteristic in dependence of rotational speeds is shown.

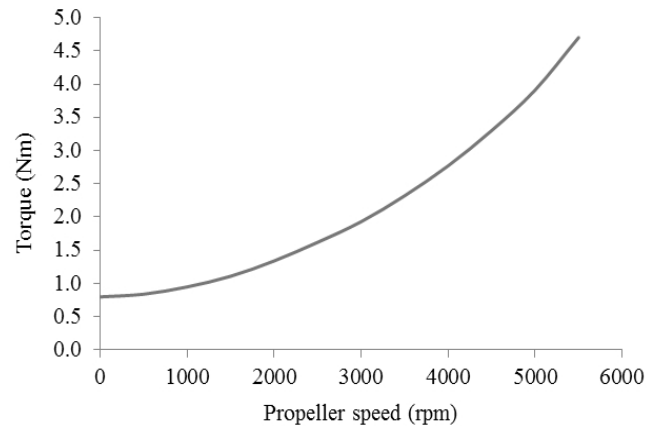


Fig. 4. Measured torque characteristic of the propeller.

ERPMSM load tests in motor operation were conducted in delta configuration to achieve more power at lower rotational speeds. Three primary supply voltages were used, $U_{DC} = 14.8, 18.5$ and 20.9 V. $U_{DC} = 14.8$ V was considered as the minimal voltage at which the rotational speed $n = 3000$ rpm was guaranteed by the specified propeller. Voltage $U_{DC} = 18.5$ V was chosen due to the nominal voltage of 5S-type batteries, which was achieved at the above-mentioned rotational speed in ERPMSMs generator mode in star connection [4]. The chosen voltage level of $U_{DC} = 20.9$ V is equivalent to the voltage output of the battery at fully charged state, at which rotational speed $n = 4000$ rpm was reachable.

While loading ERPMSM with a propeller, using nominal battery voltage $U_{DC} = 18.5$ V the rotational speed of nearly $n = 3500$ rpm was reached. Due to rapid rise from $n = 2500$ rpm the counter torque of the propeller was increasing with the supply current from the batteries. At $n = 3500$ rpm the measured supply current was $I_{DC} = 35$ A at the torque level of $T_{pr} = 1.46$ Nm.

The measured phase current values in the machine after rectification were considerably smaller than the supply currents. As previously noted, the supply voltage from the batteries was $I_{DC} = 35.0$ A. In this case the measured phase current in the machine was $I_{I3} = 16.4$ A, also the phase voltage was only $U_I = 12.2$ V_{AC}. In Fig. 5, the dependency of phase and supply voltages and phase and supply currents at different rotational speed is represented.

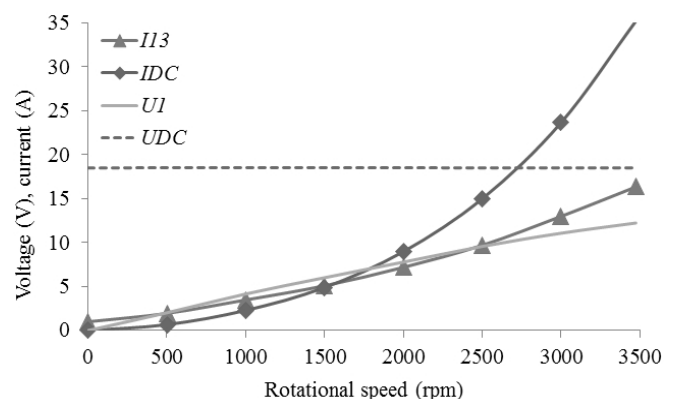


Fig. 5. Current and voltage dependencies of the rotational speed with propeller as the load.

The ratios between the incoming power to inverter P_{DC} and mechanical power P_2 measured by a torque sensor which was connected to the ERPMSM's rotor is characterized in Fig. 6.

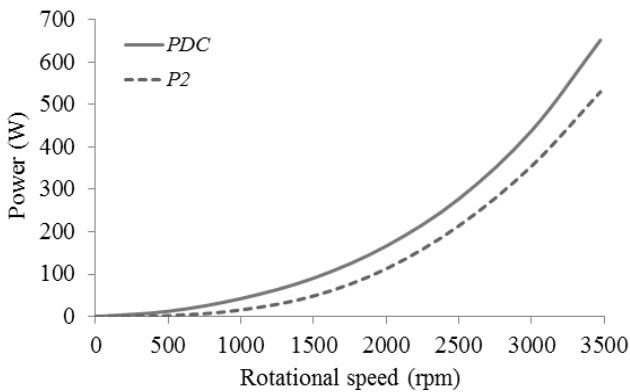


Fig. 6. The relations between the input P_{DC} and output power P_2 in dependence of the rotational speed.

The difference between P_{DC} and P_2 is an expression of the total exponential rise in power loss P_{loss} of the machine while consisting of magnetic, mechanical and residual losses. Losses in semiconductors of rectifying circuits also have a part in those losses. The most significant portion, though, is formed by ERPMSM electrical, in other words, copper losses P_{cu} , which constitute 55 % of the total loss in conditions $n = 3500$ rpm, $U_{DC} = 18.5$ V_{DC} and $I_{DC} = 35.0$ A. Almost 30 % of P_{loss} value resulted from the higher harmonics by the inverter during switching. Other losses compose of iron losses $P_{fe} = 8.0$ W, which have been previously determined [5], [6], mechanical losses P_{mech} , induced by friction in bearings and aerodynamic losses, generated by aerodynamic drag dependant on rotational speed of the rotor.

Experimental documentation of ERPMSM mechanical characteristics were conducted with the help of a specific test rig with a servo drive for loading the ERPMSM (Fig. 7), enabling torque and rotational speed measurements.

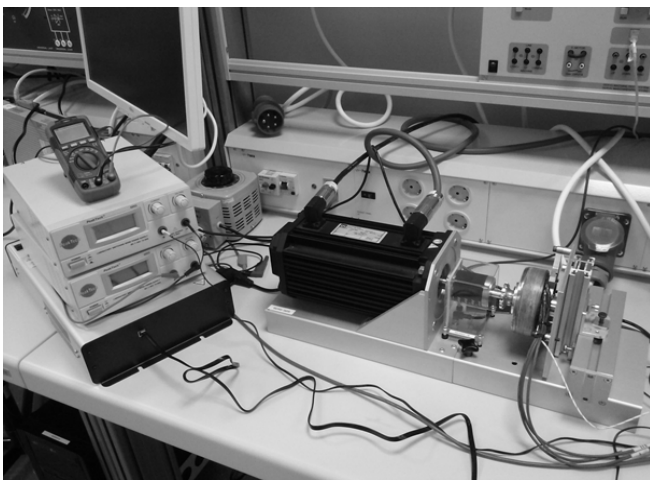


Fig. 7. Test bench of the ERPMSM.

During the load tests, servo drive was configured to be equivalent to the counter torque characteristics of the propeller.

In Fig. 8 based on propeller, the values of the dependence of the mechanical load T_m values against rotational speeds

are given.

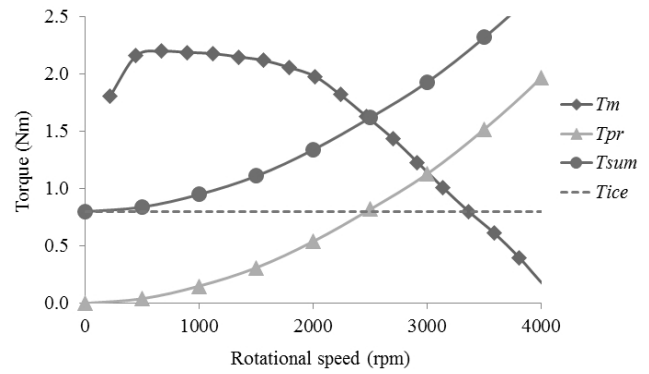


Fig. 8. Measured mechanical torque-speed characteristics at $U_{DC} = 18.5$ V.

At rated voltage $U_{DC} = 18.5$ V ERPMSM was set to rotate at the corresponding no-load speed $n_0 = 4260$ rpm. Further, the mechanically coupled servo machine was automatically increasing the load by the preliminary specified time intervals. As T_m was gradually growing during the load test, the ERPMSM's rotational speed was decreasing accordingly. This lasted until ERPMSM's torque T_m became equivalent with the counter torque resulted by the load machine. In this method ERPMSM's maximum torque $T_{max} = 2.2$ Nm at $U_{DC} = 18.5$ V and $n = 670$ rpm was measured. At rotational speed $n < 500$ rpm ERPMSM's rotor didn't have enough inertia and power anymore. This caused also the torque reduction in this part of T_m curve.

To identify the load points the counter torque curve of the propeller was included to the ERPMSM's mechanical characteristic. At rotational speed of $n = 3000$ rpm, the counter torque of the propeller was measured $T_{pr} = 1.13$ Nm. On the graph, the crossing point of T_m and T_{pr} can be noted. Correspondingly, the mechanical load torque T_m is sufficient for maintaining a stable flight regime of the UAV.

The motor operation of ERPMSM also consists of functioning as a starter, during which torque level and rotational speed must be achieved that should be sufficient for starting an ICE connected with the propeller.

According to previous measurements, the starting torque of ICE can be specified as $T_{ICE} = 0.8$ Nm [8], [9]. Additional to starting torque, propeller counter torque $T_{pr} = 1.13$ Nm at rotational speed of $n = 3000$ rpm must be taken in account. Therefore, the optimal starting torque is the sum of T_{pr} and T_{ICE} and gives a result of $T_{sum} = 1.9$ Nm. Achieving this starting torque at nominal battery voltage of $U_{DC} = 18.5$ V, the reduction in rotational speed at the starting moment was expected.

Corresponding to Fig. 8, crossing of T_m and T_{sum} curves can be observed on rotational speed of $n = 2500$ rpm. Nevertheless, for the reason that the starting interval does not exceed 3 seconds, loss in flight speed caused by loss of rotational speed can be interpreted as marginal.

In addition, in case of fully charged batteries, it would be possible to exploit higher voltages than nominal U_{DC} for starting.

In Fig. 9, on torque characteristic at $U_{DC} = 20.9$ V, at rotational speed of $n = 4000$ rpm is shown.

The rise in phase voltages ($U_l = 14.6$ V_{AC}), phase currents ($I_{l3} = 25.0$ A) and rotational speed ($n = 4000$ rpm) induces

the rise in the ERPMSMs mechanical torque up to $T_m = 2.6$ Nm.

Figure 9 depicts also the rise of counter torque of the propeller ($T_{pr} = 1.97$ Nm) at this rotational speed. Due to that the torque required to start ICE increases to $T_{sum} = 2.77$ Nm, which exceeds the maximum mechanical torque T_m .

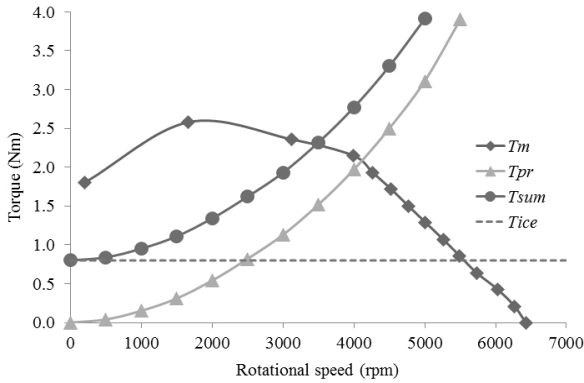


Fig. 9. Measured mechanical torque-speed characteristics at $U_{DC} = 20.9$ V.

At given conditions, the crossing of $T_{sum} = T_{pr} + T_{ICE}$ with T_m can be marked at rotational speed of $n = 3500$ rpm, which exceeds the minimal rotational speed of the propeller, required for a stable flight by 500 rpm. Therefore, the necessary flight speed is ensured even during the ICE starting period.

At ERPMSM operation as a motor, it is also used for take-offs of the UAV. Ensuring the required rate of increase in flight height, the flight speed of 80 km/h at normal atmospheric pressure must be achieved. Therefore, enough thrust must be generated by the propeller i.e. rotational speed $n = 3800$ rpm reached, without considering the UAV's aerodynamic drag.

At take-off, ICE and ERPMSM work in parallel, being mechanically coupled. Summation of both of the machines output torques T_m and T_{ICE} at various rotational speeds, based on ERPMSM maximal supply voltage $U_{DC} = 20.9$ V, and using counter torque of the propeller T_{pr} as a contrast, total output torque of the HPS $T_{sum} = 2.95$ Nm and maximal rotational speed of $n = 4860$ rpm at given conditions could be observed (Fig 10).

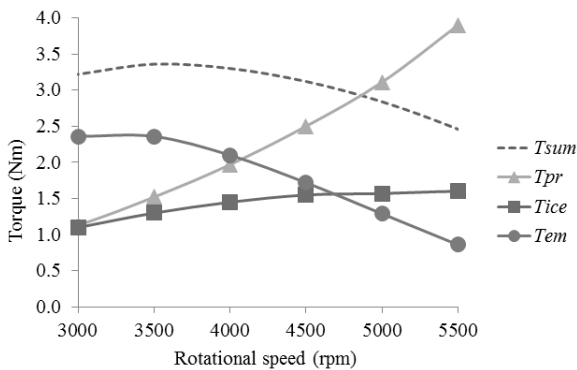


Fig. 10. Torque-speed characteristics during take-off.

At such rotational speed, theoretical flight speed in relation to earth of 103 km/h could be reached. Although, taking into account the increasing aerodynamic drag of the UAV due to increase in flight speed, the real flight speed

would be lower, but nevertheless exceeding minimal take-off speed.

IV. THERMAL CHARACTERISATION

The temperature characteristic of a PMSM expresses the nature of the temperature change during a certain amount of time and at a constant current in the stator windings. The objective of temperature tests is to determine the value of the maximum current where a PMSM reaches the maximum stabilized temperature, which is permissible to the winding insulation and to the permanent magnets [4].

The aim of the current thermal experiments was to determine the maximal temperature of ERPMSMs active parts on steady load. During the experiments, a propeller was used as a load and as a cooling element. Assuming intensive cooling by the propeller, ERPMSM could handle substantially higher supply currents than expected. The first load experiment was made using the propeller at the rotational speed of 4000 rpm and at the supply voltage of $U_{DC} = 20.9$ V, that was near to 5S batteries voltage of $U_{DC} = 21$ V at their fully charged state.

The measured supply current during the experiment reached $I_{DC} = 46.17$ A, while the phase voltage was measured $U_1 = 14.6$ V_{AC} and the phase current $I_{13} = 20.39$ A. Based on that the resulting ERPMSMs apparent power $S = 890$ VA.

At set parameters, the constant temperature of windings was stabilizing after 8 minutes i.e. 480 seconds to the temperature of $\vartheta_{p1} = 64$ °C, resulting as the time constant of $\tau \approx 120$ s. The characteristics in Fig. 11 indicate the thermal time constant τ .

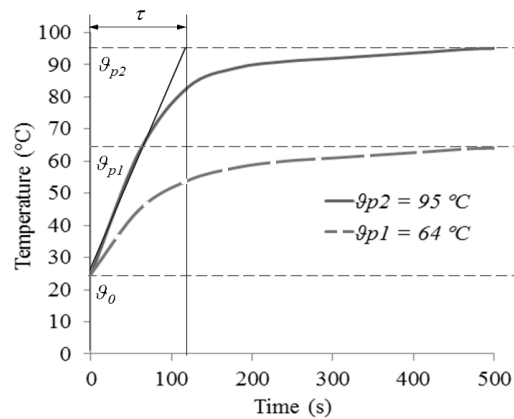


Fig. 11. Temperature characteristics with the thermal constant τ .

As the maximum temperature of the chosen magnets and winding insulations was substantially higher [10], [11], the additional experiment was made at the rotational speed of $n = 5000$ rpm, supply voltage of $U_{DC} = 27.7$ V and current of $I_{DC} = 65.6$ A. At given parameters the phase voltage $U_1 = 19.4$ V_{AC} and phase current $I_{13} = 27.6$ A, was measured, resulting the apparent power $S = 1600$ VA.

Although, at higher power, the constant temperature of $\vartheta_{p2} = 95$ °C was measured. Similarly to previous experiment the winding temperature rose to constant value during 480 seconds and gave the same time constant $\tau \approx 120$ s. The thermal time constant τ characterizes the approaching velocity rate to the final temperature, as in (1) [12]

$$\vartheta(t) = \vartheta_0 + (\vartheta_p - \vartheta_0) \left(1 - e^{-\frac{t}{\tau}} \right), \quad (1)$$

where ϑ_0 is the initial temperature (°C) and t is time (s).

The time constant τ depends mainly on the heat capacity factors and weight of ERPMSM's active materials. In practice, the final temperature is reached within 4 times of the time constant values.

The machine can be operated for an indefinite period of time only if the temperatures do not exceed specifications for each part or component of the machine [13]. Therefore, a thermal camera was used for capturing temperatures of various parts of ERPMSM, enabling comparison with results collected by use of a temperature probe. The maximum temperature in windings registered on scale was 97.3 °C, being close to the results achieved with the temperature probe.

Considering the measured temperature in windings as maximum, the temperatures of other components in the machine are lower, which ensures that in previous load conditions the allowed maximum temperatures are not exceeded either in permanent magnets.

In previous phase of the research the performed generator tests with ERPMSM were made with the maximal phase current of $I_f = 23.0$ A at rotational speed of $n = 5500$ rpm, therefore the current density in winding conductor reached up to $J = 19.3$ A/mm². The rise in temperature during the experiment stabilized at 106 °C. From the perspectives of current density and temperature, the given values are notably high. In the current case though, copper wire with the insulation rating of 180 °C (class H) is used, which has the maximum allowable current density of 23.7 A/mm² [14], resulting in even higher allowable rate. According to experiment results, the apparent power of the generator was $S = 890$ VA [4]. During the generator tests, the cooling was only provided by the impeller on the ERPMSMs external rotor.

During the experiments covered with this stage, the forced cooling by using a propeller allowed even higher phase currents I_{f3} as high as 27.6 A at rotational speed of 5000 rpm, resulting in the current density of $J = 23.2$ A/mm² and reaching to the apparent power of $S = 1600$ VA, while the winding temperature was stabilizing already at 95 °C.

The performed thermal experiments hence indicated significantly higher power and current density handling capabilities of ERPMSM with forced cooling provided by the propeller while keeping other machine active parts at notably lower constant temperatures.

V. CONCLUSIONS

Based on this experimental work it can be concluded that ERPMSM fulfils the initial requirements set as a primary propulsion element, either working in parallel with ICE or in starter mode in UAVs stable flying or in take-off regimes at the provided propeller pitch. Experimental work was performed in laboratory conditions at normal atmospheric pressure. Therefore, air mass dynamics in open air, which

make an impact on UAV flight speed, were not considered.

It was important to follow UAVs power and mass ratio or the specific power, during the research. As designed HPS exploits the electric machine with its batteries and rectifier circuits in parallel with ICE, it results in additional 1.7 kg i.e. 11 % of weight increase. These parameters were added to UAVs standard weight. Using both ERPMSM and ICE in parallel operation during the take-off, the specific power increased nearly by 71 %. On the other hand in separate performance of both ICE and ERPMSM the specific power decreased by 10 % due to the increased weight. The situation could be improved by increasing the power and torque of both machines, but as for ERPMSM this would result in larger and therefore heavier, accumulator system, which is the main reason of increase in weight of the UAV. Accordingly, the problem must be seen as complex optimization problem with objectives of keeping the mass of every element in the system as low as possible and when possible, research of advanced battery technologies, accumulation devices (super capacitors) or alternative energy resources (solar energy).

The next stage of the research includes also the reliability tests of the HPS in real life situation, mounted on the UAV. Results must be compared to theoretical calculations and with obtained experimental data.

REFERENCES

- [1] D. L. Gabriel, J. Meyer, F. du Plessis, "Brushless DC motor characterisation and selection for a fixed wing UAV", *IEEE Africon.*, Livingstone, Zambia, 2011. Online. [Available]: <http://dx.doi.org/10.1109/AFRCON.2011.6072087>
- [2] Environmental technology. Toyota official site. Online. [Available]: http://www.toyota-global.com/innovation/environmental_technology
- [3] J. R. Hendershot Jr, T. J. E. Miller, *Design of brushless permanent-magnet motors*. Ohio: Magna Physics Publishing, 2011, pp. 1.1–5.1.
- [4] R. Nukki, A. Kilk, A. Kallaste, T. Vaimann, K. Tiimus Sr, "Exterior-rotor permanent magnet synchronous machine with toroidal windings for unmanned aerial vehicles," *IEEE Electric Power Quality and Supply Reliability Conf.*, Rakvere, 2014, pp. 215–220. [Online]. Available: <https://doi.org/10.1109/pq.2014.6866813>
- [5] R. Nukki, A. Kilk, A. Kallaste, T. Vaimann, K. Tiimus Sr, "Generator mode analysis of exterior-rotor PM synchronous machine with Gramme's winding," *IEEE 5th Int. Conf. Power Engineering, Energy and Electrical Drives (POWERENG)*, Riga, 2015, pp. 347–352. [Online]. Available: <https://doi.org/10.1109/powereng.2015.7266341>
- [6] R. K. Pratapa, "Modeling and analysis of radial flux toroidally wound twin rotor permanent magnet motor", MSc. Thesis, Agricultural and Mechanical College, Louisiana State University, 2010.
- [7] Roto Motor e-shop website. Online. [Available]: <http://www.rotomotor.cz/rotomotor/eshop/4-1-Accessories>
- [8] I. H. Mengistu, "Small internal combustion engine testing for a hybrid-electric remotely-piloted aircraft" MSc. Thesis, Air Force Institute of Technology, 2011.
- [9] Honda Engines GX35 product website. Online. [Available]: <http://engines.honda.com/models/model-detail/gx35>
- [10] Arnold Magnetic Technologies. Online. [Available]: http://www.arnoldmagnetics.com/Neodymium_Literature.aspx
- [11] Broccott UK 0.355mm enamelled copper winding wire product website. Online. [Available]: <http://www.brocott.co.uk/enamelled-magnet-wire/1kg-spools/0-355mm-enamelled-copper-winding-wire-1kg-ww0355-1000.html>
- [12] H. A. Toliyat, G. B. Klimanang, *Handbook of Electric Motors*. New York: Marcel Dekker, Inc, 2004, pp. 638–639. [Online]. Available: <https://doi.org/10.1201/9781420030389>
- [13] J. F. Gieras, R. J. Wang, M. J. Kamper, *Axial flux permanent magnet brushless machines*. Springer Science, 2008, pp. 272–273. [Online]. Available: <https://doi.org/10.1007/978-1-4020-8227-6>
- [14] W. H. Yeadon, B. M. Frustaglio, "Current density", *SMTA Fall Conf.*, 2010.